mathematics

MDPI

Article

A Microscopic Heterogeneous Traffic Flow Model Considering Distance Headway

Faryal Ali [1,*], Zawar Hussain Khan [2], Khurram Shehzad Khattak [3], Thomas Aaron Gulliver [1] and Akhtar Nawaz Khan [2]

[1] Department of Electrical and Computer Engineering, University of Victoria, Victoria, BC V8W 2Y2, Canada
[2] Department of Electrical Engineering, Jalozai Campus, University of Engineering and Technology Peshawar, Jalozai 24240, Pakistan
[3] Department of Computer System Engineering, University of Engineering and Technology, Peshawar 25000, Pakistan
* Correspondence: faryalali@uvic.ca

Abstract: The intelligent driver (ID) model characterizes traffic behavior with a constant acceleration exponent and does not follow traffic physics. This results in unrealistic traffic behavior. In this paper, a new microscopic heterogeneous traffic flow model is proposed which improves the performance of the ID model. The forward and lateral distance headways are used to characterize traffic behavior. The stability of the ID and proposed models is examined over a 1000 m circular road with a traffic disturbance after 30 s. The results obtained show that the proposed model is more stable than the ID model. The performance of the proposed and ID models is evaluated over an 1800 m circular road for 150 s with a platoon of 51 vehicles. Results are presented which indicate that traffic evolves realistically with the proposed model. This is because it is based on the lateral distance headway.

Keywords: intelligent driver model; acceleration exponent; heterogeneous flow; forward and lateral distance headway

MSC: 37M05

Citation: Ali, F.; Khan, Z.H.; Khattak, K.S.; Gulliver, T.A.; Khan, A.N. A Microscopic Heterogeneous Traffic Flow Model Considering Distance Headway. *Mathematics* **2023**, *11*, 184. https://doi.org/10.3390/math11010184

Academic Editors: Babak Shiri and Zahra Alijani

Received: 25 November 2022
Revised: 23 December 2022
Accepted: 23 December 2022
Published: 29 December 2022

1. Introduction

Urban traffic congestion is a major concern in developing countries [1]. Congestion causes traffic delays, excessive fuel consumption, pollution, and safety problems [2–5]. As urban populations increase, so does the number of vehicles [6]. In these areas, vehicles utilize vacant road space and lane discipline is often ignored, resulting in heterogeneous traffic [7]. The distance covered by a vehicle to align to forward vehicles in a lane is known as the forward distance headway, and the lateral distance between vehicles is called the lateral distance headway. These headways affect driver response and cause traffic flow variations [8]. Vehicles in heterogeneous traffic adjust their position and speed based on the lateral distance headway. Thus, the realistic characterization of heterogeneous traffic requires a model that considers this headway and lane-changing behavior.

Three types of models are employed for traffic flow characterization: microscopic, macroscopic, and mesoscopic. Microscopic models consider individual vehicle behavior and are often based on driver physical and psychological responses [9]. These models employ parameters such as vehicle position, velocity, and time and distance headways [10]. They are used to predict vehicle dynamics [6]. Macroscopic models consider aggregate vehicle behavior [11], whereas mesoscopic models take into account both individual and aggregate behavior [12].

Gazis et al. [13] developed a microscopic model which considers driver response to forward traffic conditions based on the velocity difference. Drivers adjust their speed with a constant delay of 1.3 s, so driver behavior due to traffic conditions is ignored. Newell [14]

proposed a model for vehicle behavior in dense traffic. Velocity is based on the distance headway, so a larger distance headway results in a lower density and, hence, a greater velocity. However, this relationship results in high acceleration, which is not realistic [15]. Moreover, this model neglects variations in driver behavior as a constant time headway is employed [16].

Bando et al. [17] improved the Newell model but neglected velocity differences resulting in unstable behavior. Moreover, deviations from the equilibrium velocity result in high acceleration, which is not realistic. Further, small distances between vehicles occur, which can result in accidents. Helbing and Tilch [18] developed a model which considers the reaction to velocity differences and, thus, accurately characterizes the time headway and velocity during congestion. However, acceleration occurs over a short time, which is typical of an aggressive driver, so slow and average driver behavior is neglected. Gipps [19] proposed a model based on driver response to forward traffic with realistic acceleration. However, this model is only suitable for a small range of parameters.

Treiber, Henneck, and Helbing [15] developed the intelligent driver (ID) model based on driver response. With this model, driver behavior is based on the velocity and distance headway of forward vehicles, and typical traffic parameters are employed [20–22]. However, the acceleration exponent, δ, in the ID model is a constant and so cannot characterize driver behavior under different traffic conditions. To improve the ID model for intersections, driver response based on deceleration has been incorporated [23]. However, the distance between vehicles is small at high velocities, which can result in accidents. This distance can be adjusted using parameters based on velocity [24]. The ID model has been used to characterize connected and autonomous vehicles (CAVs) [25,26]. However, this model does not provide realistic CAV behavior for real traffic conditions [27].

A model integrating psychoticism, extraversion, and neuroticism (PEN) was proposed in [28] for heterogeneous traffic. However, this model ignores traffic physics, so the results can be unrealistic. A microscopic car-following model for CAVs in heterogeneous traffic was proposed in [29] to mitigate oscillations and improve traffic flow. However, this model is complex and so is difficult to implement. A traffic model based on distance headway was developed in [30], but a constant lateral distance headway is used, which is unrealistic [7].

Gunay [31] proposed a model which characterizes non-lane-based traffic considering the positions of leading vehicles. However, heterogeneous traffic and lane discipline are ignored [32]. In heterogeneous traffic, vehicles interact both longitudinally and laterally and are strongly correlated [7]. Moreover, the road capacity is higher with heterogeneous traffic due to the gap-filling behavior [33] as shown in Figure 1. Lane changes increase acceleration and deceleration and can result in stop-and-go traffic behavior [34] and increase the probability of accidents [35].

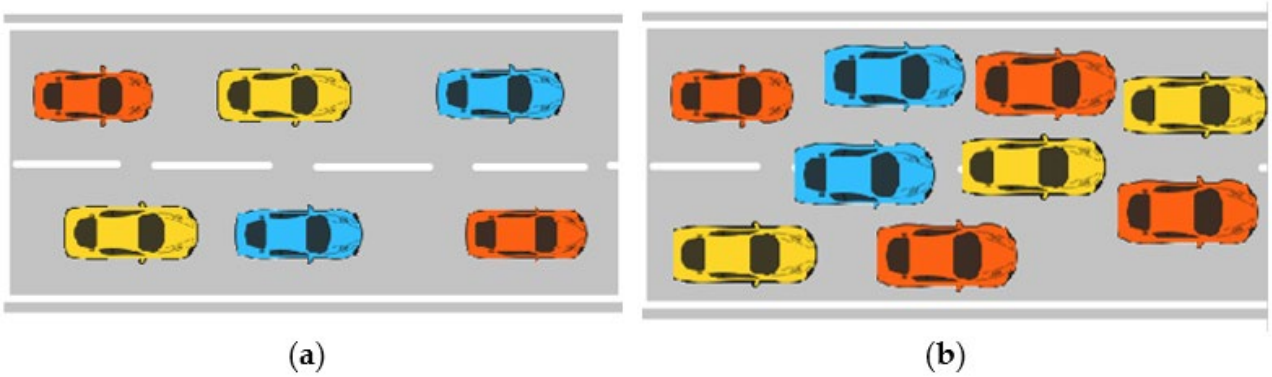

Figure 1. (**a**) Lane-based homogenous traffic. (**b**) Non-lane-based heterogeneous traffic with gap-filling behavior.

In this paper, a new microscopic heterogeneous traffic model is proposed which characterizes traffic behavior based on the forward and lateral distance headways. The

performance of the ID and proposed models is evaluated over an 1800 m circular road for 150 s, and the stability is examined over a 1000 m circular road for 120 s. A shorter duration is used for the stability analysis as this is sufficient to evaluate model behavior. The results obtained indicate that traffic behavior with the proposed model is more realistic.

The remainder of this paper is organized as follows. The ID and proposed models are discussed in Section 2, and Section 3 presents the stability analysis. The performance of these models is investigated in Section 4. Finally, Section 5 gives some concluding remarks.

2. Traffic Flow Models

The ID model is a microscopic model that presumes forward traffic conditions [36]. It characterizes acceleration based on driver response, the distance between vehicles, and the time required to align to forward vehicles. According to this model, driver response is based on the ratio of average velocity to maximum velocity. Acceleration depends on this ratio and traffic flow is smooth when this ratio is 1.

The ID model acceleration is given by [15]:

$$\frac{dv}{dt} = a_{max}\left(1 - \left(\frac{v}{v_0}\right)^{\delta} - \left(\frac{H}{s}\right)^{2}\right), \tag{1}$$

where a_{max} is the maximum acceleration, v_0 is the maximum velocity, v is the average velocity, and s is the bumper-to-bumper distance between vehicles. H is the distance headway covered during traffic alignment, which can be expressed as [15]:

$$H = J + Tv + \frac{v\Delta v}{2\sqrt{a_{max}a_{min}}} \tag{2}$$

where J is the traffic jam spacing, T is the time headway, a_{min} is the maximum acceleration, and Δv is the difference in velocity between the following and leading vehicles.

The ID model characterizes driver response based on an acceleration exponent, δ, which is a constant. This constant must represent driver behavior for a variety of traffic conditions. However, it does not follow traffic flow physics and, thus, can result in unrealistic behavior. Therefore, an acceleration exponent based on heterogeneous traffic is proposed to better characterize traffic.

In heterogeneous traffic, driver response is based on the forward and lateral distance headways as well as lane-changing behavior and is given by:

$$\delta = \frac{\Delta v d_1}{a^2 \rho} \tag{3}$$

where Δv is the difference in velocity between the following and leading vehicles, which characterizes lane changes and traffic alignment during these changes. ρ is the traffic density, d_1 is the distance headway between the following and leading vehicles as shown in Figure 2, and a is the lateral distance headway. A driver reacts to perceived conditions and aligns with the forward and adjacent vehicles. The reaction is quick for a small distance headway as alignment occurs over a short distance and vice versa for a longer distance headway. In other words, vehicle movement is greater with a larger distance headway.

In heterogeneous traffic, the lateral distance headway varies and is small during congestion. Further, when the traffic density is large, the forward distance headway, h, is small, so:

$$\rho = \frac{1}{h} \tag{4}$$

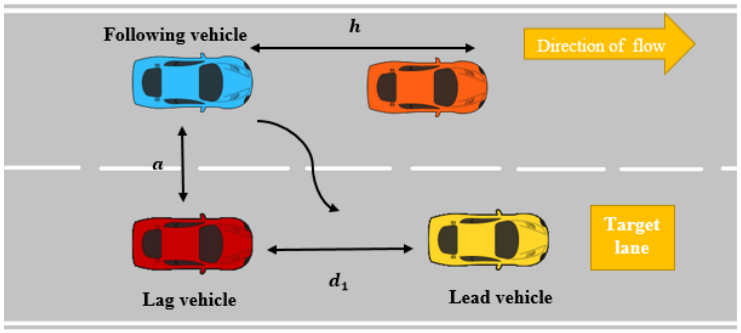

Figure 2. Heterogeneous traffic with lane changing.

Substituting (4) in (3) we have:

$$\delta = \frac{\Delta v d_1 h}{a^2} \tag{5}$$

and replacing δ in (1) with this expression gives the proposed model:

$$\frac{dv}{dt} = a_{max}\left(1 - \left(\frac{v}{v_0}\right)^{\frac{\Delta v d_1 h}{a^2}} - \left(\frac{H}{s}\right)^2\right) \tag{6}$$

This model characterizes heterogeneous traffic based on the forward and lateral distance headways. It is better than the ID model because it is based on traffic conditions rather than on a number, which is a compromise to fit all conditions.

For microscopic models, traffic density is given by $D = \frac{1}{s_e}$ [37] where s_e is the distance headway at equilibrium. At equilibrium, $\Delta v = 0$, so from (2):

$$s_e = (J + Tv)\left(1 - \left(\frac{v}{v_0}\right)^{\delta}\right)^{-1/2} \tag{7}$$

For the proposed model, the equilibrium distance headway is:

$$s_e = (J + Tv)\left(1 - \left(\frac{v}{v_0}\right)^{\frac{\Delta v d_1 h}{a^2}}\right)^{-1/2} \tag{8}$$

Equation (7) shows that the equilibrium distance headway for the ID model is based on a constant exponent which is the same for all traffic conditions. Conversely, this headway for the proposed model (8) is based on heterogeneous traffic parameters and is not a constant.

Traffic flow is the product of velocity and density, $f = \frac{v}{s_e}$ [20], so the flow for the ID model is:

$$f = \frac{v}{(J + Tv)\left(1 - \left(\frac{v}{v_0}\right)^{\delta}\right)^{-1/2}}, \tag{9}$$

Substituting the proposed acceleration exponent term, the traffic flow for the proposed model is:

$$f = \frac{v}{(J + Tv)\left(1 - \left(\frac{v}{v_0}\right)^{\frac{\Delta v d_1 h}{a^2}}\right)^{-1/2}}. \tag{10}$$

This flow is based on heterogeneous traffic parameters and so is more realistic than the flow for the ID model.

3. Stability Analysis

The stability of the ID and proposed models is evaluated over a 1000 m circular road for 120 s. The value of the acceleration exponent ranges from 1 to ∞ and is typically 4 [15]. Typical values of the lateral distance headway are in the range of 0.5 m to 2.2 m [38]. Hence, the ID model is evaluated for $\delta = 1,\ 4,\ 10$, and 30 and the proposed model for $a = 0.5,\ 0.6,\ 1,\ 1.5,\ 2$, and 2.2 m. The leading vehicle velocity is 33.3 m/s and the following vehicle velocity is 30 m/s, so $\Delta v = 33.3 - 30 = 3.3$ m/s. The distance headway, d_1, varies between 0.04 m and 117.9 m [39], and here it is set to 0.1 m. The initial equilibrium velocity is 6 m/s and the number of vehicles on the road is 51. The disturbance is induced at 30 s at the maximum acceleration of 1.67 m/s^2. The stability analysis parameters are given in Table 1.

Table 1. Stability analysis parameters.

Parameter	Value
Initial equilibrium velocity	6 m/s
Time headway, T	0.8 s
Forward distance headway, h	5 m
Velocity difference between the following and leading vehicles, Δv	3.3 m/s
Distance headway between the following and leading vehicles, d_1	0.1 m
Jam spacing, J	2 m
Maximum acceleration, a_{max}	1.4 m/s^2
Maximum deceleration, a_{min}	1.67 m/s^2
Vehicle length, L	5 m
Time step, Δt	0.5 s
Acceleration exponent, δ	1, 4, 10 and 30
Lateral distance headway, a	0.5, 0.6, 1, 1.5, 2, and 2.2 m

The velocity evolution of the ID and proposed models is given in Figure 3. The red line is the trajectory of the 1st vehicle and the black lines are the trajectories of the following 50 vehicles. For the ID model, with $\delta = 1$, the velocity of the 1st vehicle suddenly drops to 5.1 m/s at 30 s and then increases to 6.2 m/s at 34 s and starts to oscillate. At 80 s, the velocity oscillates between 5.7 m/s and 6.4 m/s, and at 119 s, the velocity oscillates between 5.3 m/s and 6.6 m/s, as shown in Figure 3a. With $\delta = 4$, the velocity of the 1st vehicle suddenly drops to 5.1 m/s at 30 s and then increases to 6.3 m/s at 33 s and starts to oscillate. At 85 s, the velocity oscillates between 5.0 m/s and 7.0 m/s, and at 120 s, it oscillates between 2.6 m/s and 9.0 m/s, as shown in Figure 3b. With $\delta = 10$, the velocity of the 1st vehicle suddenly drops to 5.1 m/s at 30 s and then increases to 6.3 m/s at 33 s and starts to oscillate. At 88 s, the velocity oscillates between 4.9 m/s and 7.2 m/s, and at 120 s, the velocity oscillates between 2.6 m/s and 9.1 m/s, as shown in Figure 3c. With $\delta = 30$, the velocity of the 1st vehicle suddenly drops to 5.1 m/s at 30 s and then increases to 6.3 m/s at 33 s and starts to oscillate. At 88 s, the velocity oscillates between 4.9 m/s and 7.2 m/s, and at 120 s, the velocity oscillates between 2.6 m/s and 9.1 m/s, as shown in Figure 3d.

For the proposed model, with $a = 0.5$ m, the velocity of the 1st vehicle suddenly drops to 5.1 m/s at 30 s and then increases to 6.3 m/s at 33.5 s and starts to oscillate. At 85 s, the velocity oscillates between 5.0 m/s and 7.1 m/s, and at 119 s, the velocity oscillates between 2.7 m/s and 8.9 m/s, as shown in Figure 3e. With $a = 0.6$ m, the velocity of the 1st vehicle suddenly drops to 5.1 m/s at 30 s and then increases to 6.3 m/s at 33.5 s and starts to oscillate. At 83 s, the velocity oscillates between 5.2 m/s and 7.0 m/s, and at 119.5 s, the velocity oscillates between 2.7 m/s and 8.9 m/s, as shown in Figure 3f. With $a = 1$ m, the velocity of the 1st vehicle suddenly drops to 5.1 m/s at 30 s and then increases to 6.2 m/s at 33.5 s and starts to oscillate. At 82 s, the velocity oscillates between 5.5 m/s and 6.6 m/s, and at 119.5 s, the velocity oscillates between 4.4 m/s and 7.2 m/s, as shown in Figure 3g. With $a = 1.5$ m, the velocity of the 1st vehicle suddenly drops to 5.2 m/s at 30 s and then increases to 6.3 m/s at 34.5 s and starts to oscillate. At 80 s, the velocity oscillates between 5.8 m/s and 6.3 m/s, and at 120 s, the velocity oscillates between 5.4 m/s

and 6.5 m/s, as shown in Figure 3h. With $a = 2$ m, the velocity of the 1st vehicle suddenly drops to 5.19 m/s at 30 s and then increases to 6.2 m/s at 36 s and starts to oscillate. At 82 s, the velocity oscillates between 5.8 m/s and 6.4 m/s, and at 119 s, the velocity oscillates between 5.5 m/s and 6.5 m/s, as shown in Figure 3i. With $a = 2.2$ m, the velocity of the 1st vehicle suddenly drops to 5.2 m/s at 30 s and then increases to 6.2 m/s at 37 s and starts to oscillate. At 80 s, the velocity oscillates between 5.7 m/s and 6.4 m/s, and at 120 s, the velocity oscillates between 6.4 m/s and 6.6 m/s, as shown in Figure 3j.

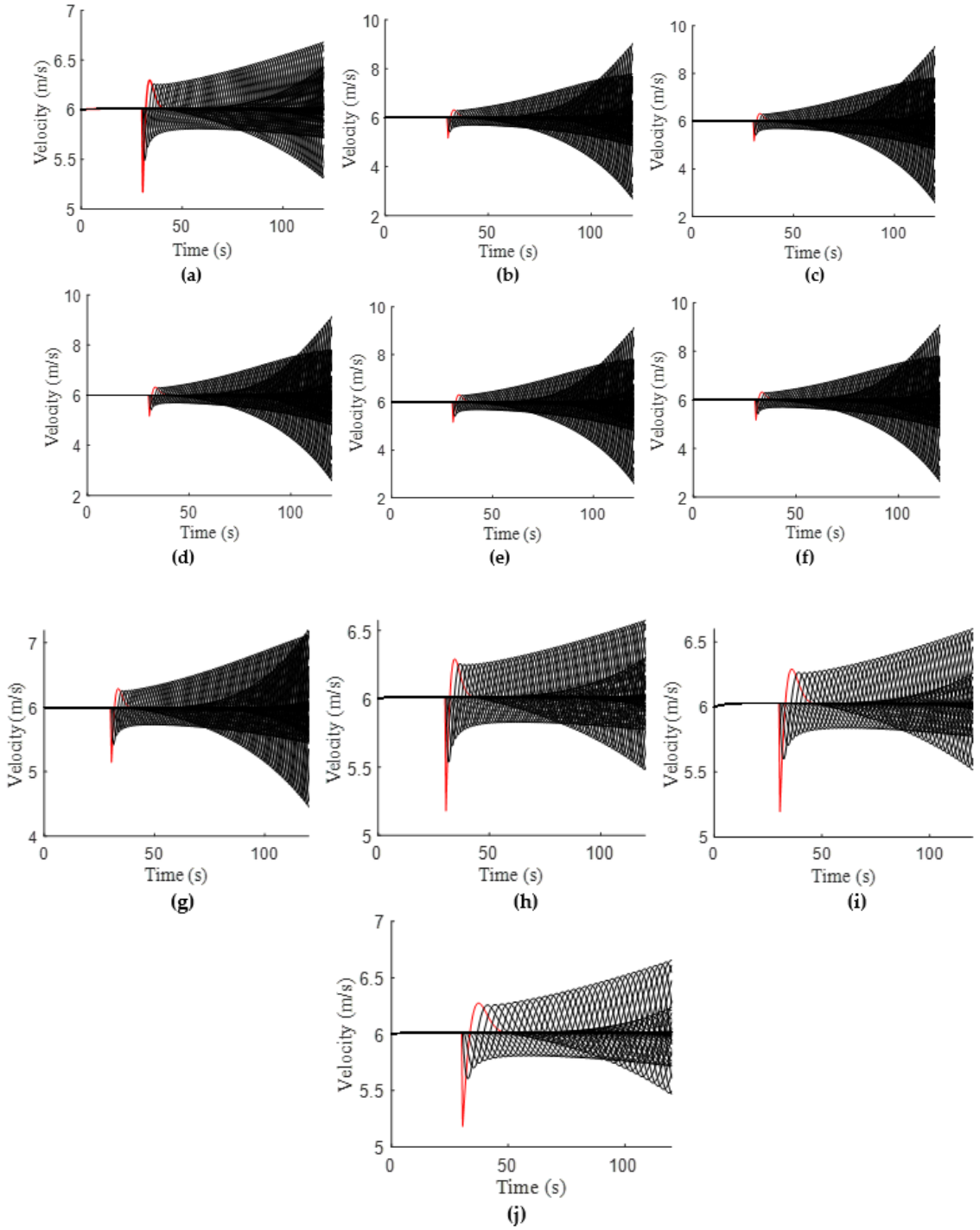

Figure 3. Velocity evolution of the ID and proposed models with an initial equilibrium velocity of 6 m/s: (**a**) $\delta = 1$; (**b**) $\delta = 4$; (**c**) $\delta = 10$; (**d**) $\delta = 30$; (**e**) $a = 0.5$ m; (**f**) $a = 0.6$ m; (**g**) $a = 1$ m; (**h**) $a = 1.5$ m; (**i**) $a = 2$ m; (**j**) $a = 2.2$ m.

The time and space evolution of the vehicles for the ID and proposed models is given in Figure 4. This shows vehicle mobility and stop-and-go behavior due to congestion. Both models produce stop-and-go waves after a few seconds. For the ID model, from $\delta = 1$ to $\delta = 10$, an increase in δ increases the stop-and-go waves produced over time and space, and above $\delta = 10$, the behavior is similar to that for $\delta = 10$, as shown in Figure 4a–d. Conversely, for the proposed model, the stop-and-go waves produced decrease as the lateral distance headway increases.

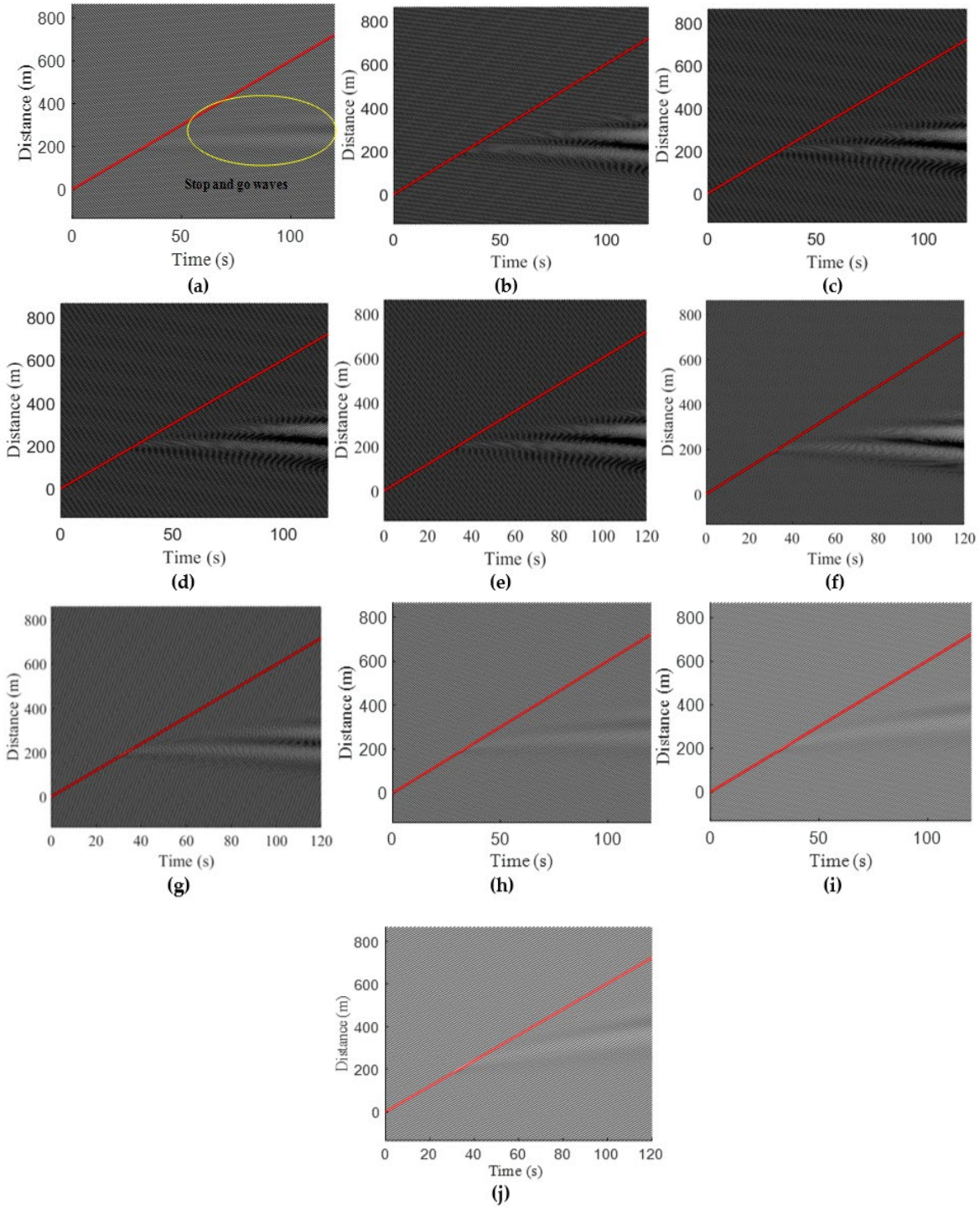

Figure 4. Spatio-temporal performance of the ID and proposed models over a 1000 m circular road: (**a**) $\delta = 1$; (**b**) $\delta = 4$; (**c**) $\delta = 10$; (**d**) $\delta = 30$; (**e**) $a = 0.5$ m; (**f**) $a = 0.6$ m; (**g**) $a = 1$ m; (**h**) $a = 1.5$ m; (**i**) $a = 2$ m; (**j**) $a = 2.2$ m.

These results show that with the ID model, as δ increases from 1 to 10, the velocity oscillations increase as indicated in Figure 3a–c, but above $\delta = 10$, these oscillations are similar. This unstable and unrealistic behavior occurs because of the constant exponent. With the proposed model, as the lateral distance headway increases the velocity oscillations decrease over time. This behavior is more stable and realistic than the ID model because the proposed model is based on real traffic parameters. Furthermore, with the proposed model, the traffic is smooth as the stop-and-go waves produced are based on the lateral distance headway and decrease with an increase in this headway, as shown in Figure 4.

4. Performance Results

In this section, the performance of the proposed and ID models is evaluated over a circular road of length 1800 m for 150 s using the Euler technique with a time step of 0.5 s [37]. The simulation parameters are given in Table 2. The forward distance headway is 5 m [40]. The lateral distance headway is typically between 0.5 m and 2.2 m [38], so here 0.5, 0.6, 1, 1.5, 2, and 2.2 m are used. The difference in velocity for the proposed model is $\Delta v = 33.3 - 30 = 3.3$ m/s. The distance headway, d_1, typically varies between 0.04 m and 117.9 m [39], so here it is set to 0.1 m. The acceleration exponent ranges from 1 to ∞ and is typically 4 [15], so here 1, 4, 10, and 30 are used. The maximum normalized density at $v = 0$ m/s is $\frac{1}{J} = 0.5$. There are 51 vehicles on the road which was obtained by dividing the road length by s_e.

Table 2. Simulation parameters.

Parameter	Value
Maximum velocity, v_0	33.3 m/s
Average velocity, v	25 m/s
Time headway, T	0.8 s
Jam spacing, J	2 m
Maximum deceleration, a_{min}	1.67 m/s^2
Maximum acceleration, a_{max}	1.4 m/s^2
Lateral distance headway, a	0.5, 0.6, 1, 1.5, 2, and 2.2 m
Forward distance headway, h	5 m
Velocity difference between the following and leading vehicles, Δv	3.3 m/s
Distance headway between the following and leading vehicles, d_1	0.1 m
Time step, Δt	0.5 s
Acceleration exponent, δ	1, 4, 10 and 30
Maximum normalized density, $\rho_m = \frac{1}{J}$ at $v = 0$ m/s	0.5
Vehicle length, l	5 m

Figure 5 presents the flow and velocity behavior of the ID and proposed models. The results are summarized in Tables 3 and 4. For the ID model, with $\delta = 1$, the maximum flow is 0.83 veh/s at density 0.08, and the corresponding critical velocity is 9.90 m/s. With $\delta = 4$, the maximum flow is 1.05 veh/s at density 0.06, and the critical velocity is 16.0 m/s. With $\delta = 10$ and 30, the maximum flow is 1.11 veh/s and 1.14 veh/s, respectively, at density 0.04, and the critical velocity is 23.3 m/s. Table 3 shows that as δ increases, the maximum flow also increases, and the maximum density between $\delta = 1$ and 10 decreases with δ and is similar for values above $\delta = 10$. The critical velocity between $\delta = 1$ and 10 increases with δ, whereas above $\delta = 10$, it is similar.

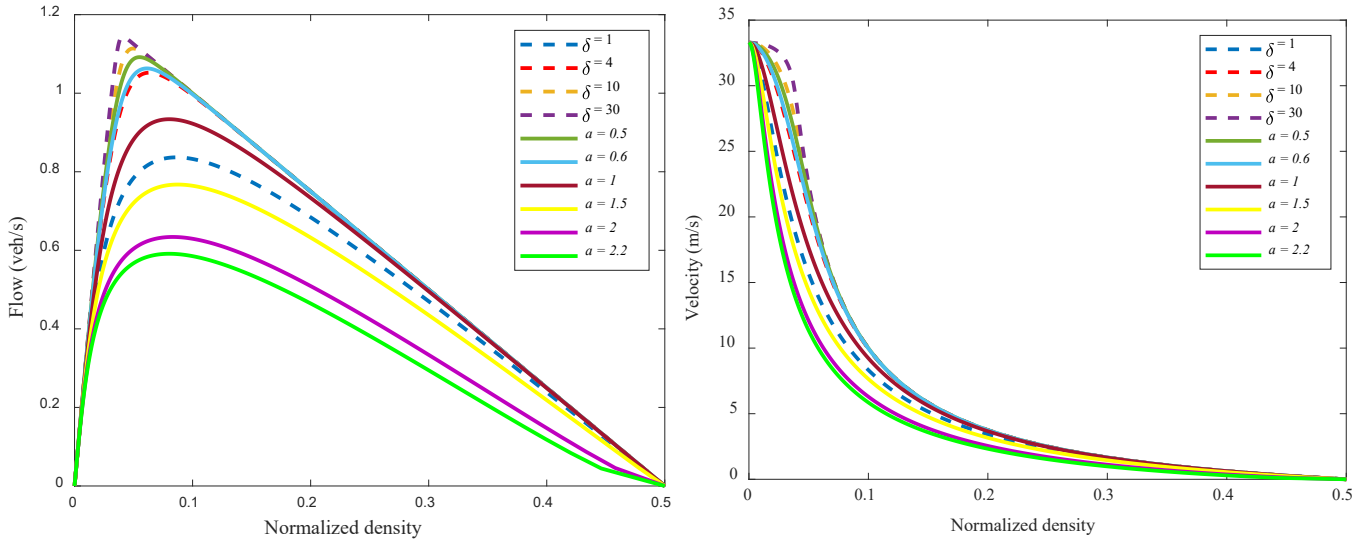

Figure 5. Flow and velocity of the ID and proposed models.

Table 3. Maximum flow, density, and critical velocity for the ID model.

Acceleration Exponent δ	Maximum Flow (veh/s)	Maximum Density	Critical Velocity (m/s)
1	0.83	0.08	9.90
4	1.05	0.06	16.0
10	1.11	0.04	23.2
30	1.14	0.04	23.2

Table 4. Maximum flow, density, and critical velocity for the proposed model.

Lateral Distance Headway, a (m)	Maximum Flow (veh/s)	Maximum Density	Critical Velocity (m/s)
0.5	1.09	0.05	19.8
0.6	1.06	0.06	18.0
1	0.93	0.08	11.8
1.5	0.76	0.09	8.70
2	0.63	0.08	7.40
2.2	0.59	0.07	7.50

For the proposed model, with $a = 0.5$ m, the maximum flow is 1.09 veh/s at density 0.05, and the critical velocity is 19.8 m/s. With $a = 0.6$ m and 1 m, the maximum flow is 1.06 veh/s and 0.93 veh/s at densities 0.06 and 0.08, respectively. The corresponding critical velocities are 18.0 m/s and 11.8 m/s, respectively. With $a = 1.5$ m and 2 m, the maximum flow is 0.76 veh/s and 0.63 veh/s at densities 0.09 and 0.08, respectively. The corresponding critical velocities are 8.70 m/s and 7.40 m/s, respectively. With $a = 2.2$ m, the maximum flow is 0.59 veh/s at density 0.07, and the critical velocity is 7.50 m/s. Table 4 shows that as the lateral distance headway increases, the maximum flow decreases, and the maximum density increases between $a = 0.5$ and 1.5 m but decreases above $a = 1.5$. The critical velocity decreases between $a = 0.5$ and 2 m but increases for $a = 2.2$ m.

The spatio–temporal evolution of the queue caused due to congestion for the ID model is given in Figure 6, and the results are summarized in Table 5. This shows that the velocity during the queue is zero. For the ID model with $\delta = 1$, the queue dissolves at 64 s, as shown in Figure 6a, and the velocity after the queue is 15.4 m/s at 89.5 s. With $\delta = 4$, the queue dissolves at 64 s, as shown in Figure 6b, and the velocity after the queue is 18.2 m/s at 93.0 s. With δ = 10 and 30, the queue occurs between 0 s and 63.50 s. The velocity after

the queue dissolves is 4.70 m/s at 66 s, and gradually decreases to 2.70 m/s at 122 s. The queue develops again at 123.5 s and lasts until 150 s between 40.0 m and 46.6 m, as shown in Figure 6c,d. For δ between 1 and 4, the maximum velocity increases with δ, but above $\delta = 4$, it is similar, as shown in Figure 6a–d.

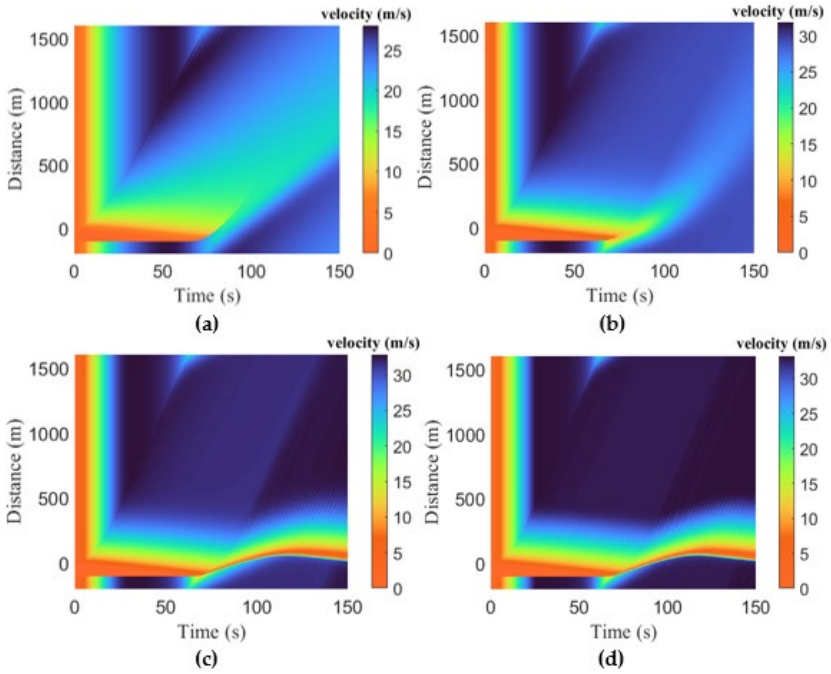

Figure 6. Velocity evolution over time and space for the ID model on an 1800 m circular road: (**a**) $\delta = 1$; (**b**) $\delta = 4$; (**c**) $\delta = 10$; (**d**) $\delta = 30$.

Table 5. Velocity and time for the ID model during and after congestion.

Acceleration Exponent, δ	Time for Which Congestion Occurs (s)	Velocity after Congestion (m/s)	Time of Velocity after Congestion (s)
1	0–64	15.4	89.5
4	0–64	18.2	93.0
10	0–63.5 and 123.5–150	4.70–2.70	66–122
30	0–63.5 and 123–150	4.70–2.70	66–122

The spatio–temporal evolution of the queue due to congestion for the proposed model is given in Figure 7 and the results are summarized in Table 6. This shows that the velocity during the queue is zero. For the proposed model, with $a = 0.5$ m, the queue exists between 0 s and 61 s. The velocity after the queue dissolves varies between 1.17 m/s at 62.5 s and 1.70 m/s at 125.5 s. The queue develops again at 127 s and lasts until 150 s between 93.2 m and 96.5 m, as shown in Figure 7a. With $a = 0.6$ m and 1 m, the queue dissolves at 61.5 s and 61.0 s, respectively, as shown in Figure 7b,c. The velocity after the queue dissolves with $a = 0.6$ m is 12.1 m/s and with $a = 1$ m is 17.7 m/s at 80.5 s and 83.5 s, respectively. With $a = 1.5$ m and 2 m, the queue dissolves at 60.5 s and 78.5 s, respectively, as shown in Figure 7d,e. The velocity after the queue dissolves with $a = 1.5$ m is 15.3 m/s and with $a = 2$ m is 9.0 m/s at 99.5 s and 102 s, respectively. With $a = 2.2$ m, the queue dissolves at 88.5 s, as shown in Figure 7f, and the velocity after the queue is 8.08 m/s at 116 s. Figure 7a–f indicate that as the lateral distance headway increases, the maximum velocity decreases.

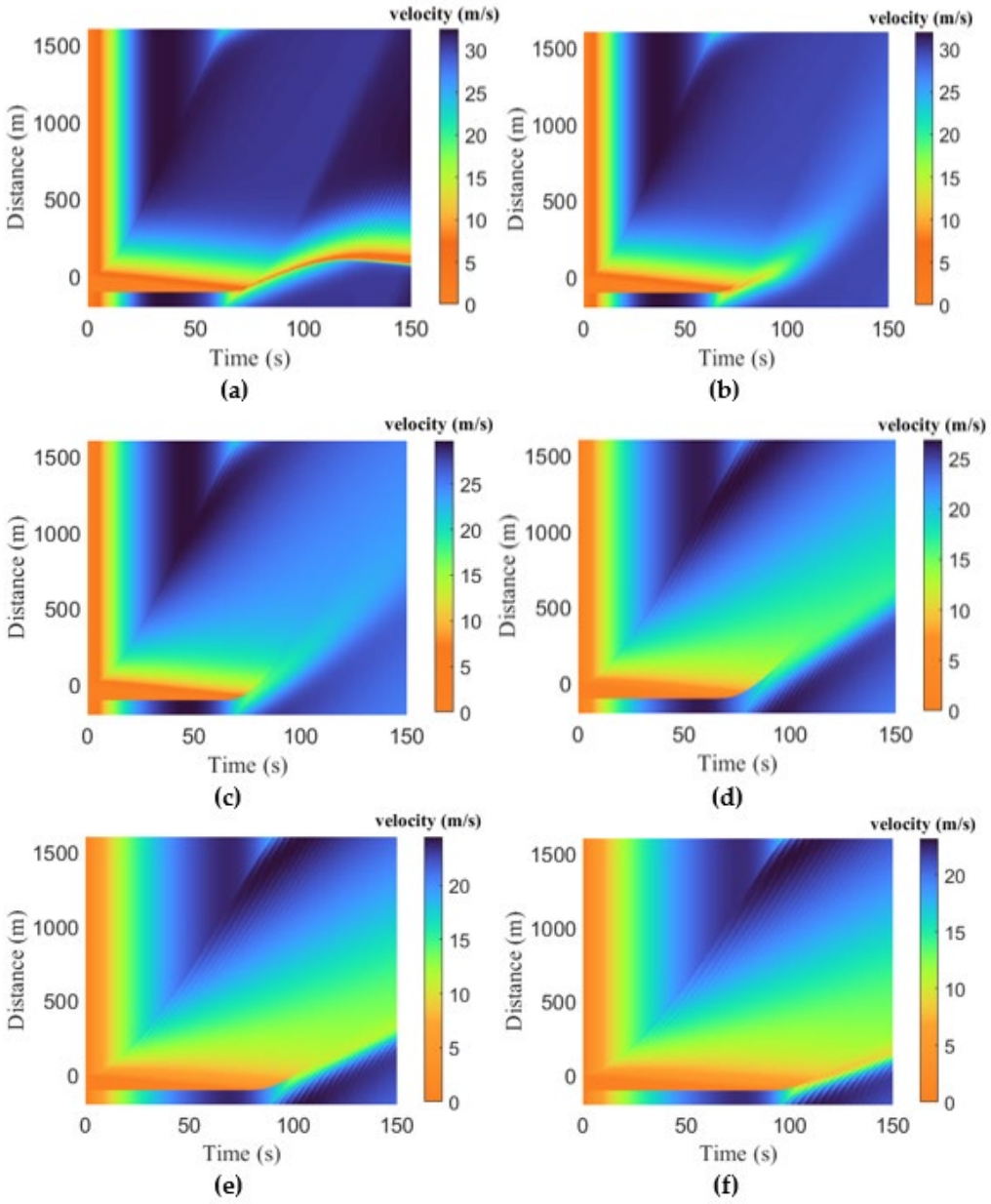

Figure 7. Velocity evolution over time and space for the proposed model on an 1800 m circular road: (**a**) $a = 0.5$ m; (**b**) $a = 0.6$ m; (**c**) $a = 1$ m; (**d**) $a = 1.5$ m; (**e**) $a = 2$ m; (**f**) $a = 2.2$ m.

Table 6. Velocity and time for the proposed model during and after congestion.

Lateral Distance Headway, a	Time for Which Congestion Occurs (s)	Velocity after Congestion (m/s)	Time of Velocity after Congestion (s)
0.5	0–61 and 127–150	1.17–1.70	62.5–125.5
0.6	0–61.5	12.1	80.5
1	0–61.0	17.7	83.5
1.5	0–60.5	15.3	99.5
2	0–78.5	9.00	102
2.2	0–88.5	8.08	116

Figure 8 presents the time and space vehicle trajectories of a platoon of 51 vehicles over an 1800 circular road for the ID model. The initial average velocity of the platoon is 25 m/s. The green trajectory is the 1st vehicle that begins to move at 0 s, whereas the black

trajectories are of the following 50 vehicles. With $\delta = 1$ and 4, the traffic queue appears for 64 s, as shown in Figure 8a,b, i.e., the 51st vehicle is in the queue for 64 s. With $\delta = 10$, the initial queue appears for 63.5 s. The 1st vehicle is in the queue for 0.5 s at 3.33 m and the last vehicle is in the queue for 63.5 s at -99.9 m. The queue appears again at 123.5 s and lasts until 150 s between 40.0 m and 46.6 m, respectively, as shown in Figure 8c. With $\delta = 30$, the initial queue appears for 63.5 s. The 1st vehicle is in the queue for 0.5 s at 3.33 m and the last vehicle is in the queue for 63.5 s at -99.9 m. The queue appears again at 123.5 s and lasts until 150 s between 40.0 m and 46.6 m, respectively, as shown in Figure 8d.

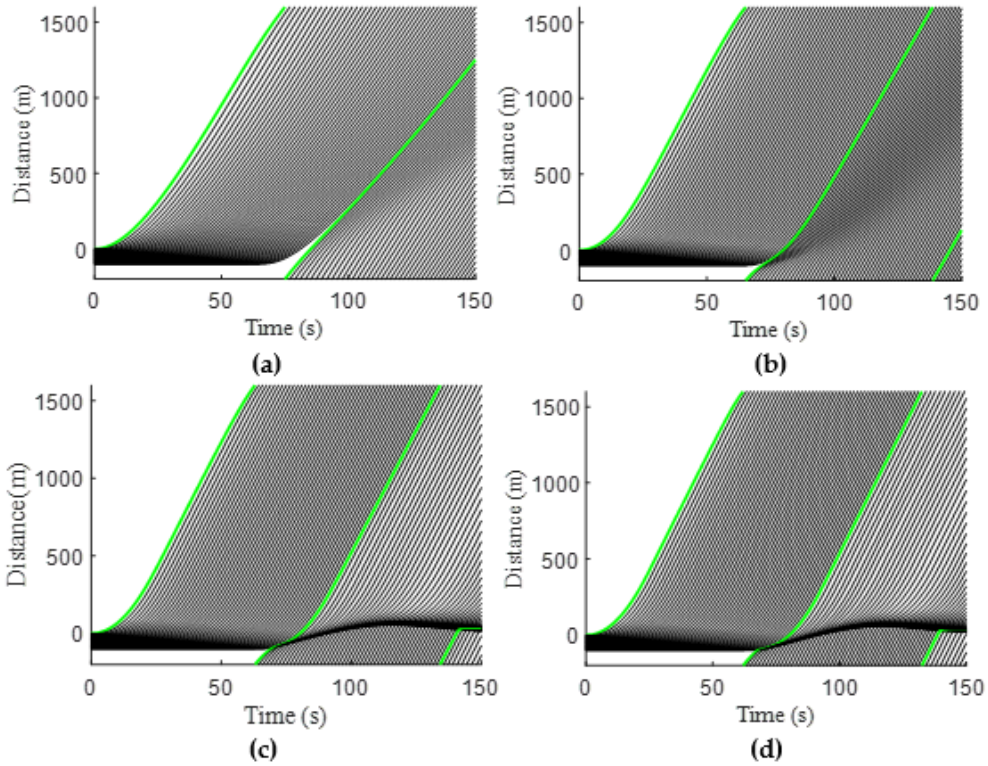

Figure 8. Time–space vehicle trajectories for the ID model over an 1800 m circular road: (**a**) $\delta = 1$; (**b**) $\delta = 4$; (**c**) $\delta = 10$; (**d**) $\delta = 30$. The colored line shows the trajectory of the first vehicle.

The positions of the 1st, 30th, and 40th vehicles at 60 s are given in Table 7. With $\delta = 1$, the position of the 1st vehicle is 1230 m, whereas the positions of the 30th and 40th vehicles are 141.0 m and -57.6 m, respectively. With $\delta = 4$, the position of the 1st vehicle is 1475 m, whereas the positions of the 30th and 40th vehicles are 137.1 m and -72.3 m, respectively. With $\delta = 10$, the position of the 1st vehicle is 1529 m, whereas the positions of the 30th and 40th vehicles are 207.0 m and -63.2 m, respectively. With $\delta = 30$, the position of the 1st vehicle is 1553 m, whereas the positions of the 30th and 40th vehicles are 173.0 m and -52.2 m, respectively. Table 7 indicates that as δ increases, the distance traveled by the 1st vehicle increases. The distance traveled by the 30th and 40th vehicles decreases between $\delta = 1$ and 4, and increases between $\delta = 4$ and 10. Above $\delta = 10$, the distance traveled again decreases.

Figure 9 presents the time and space vehicle trajectories for the proposed model. With $a = 0.5$ m, the initial queue appears for 61 s. The 1st vehicle is in the queue for 1 s at 0.6 m and the last vehicle is in the queue for 61 s at -99.9 m. The queue appears again at 127 s and lasts until 150 s between 93.2 m and 96.5 m, respectively, as shown in Figure 9a. With $a = 0.6$ and 1 m, the queue appears for 61.5 s and 61 s, respectively, as shown in Figure 9b,c, so the 51st vehicle is in the queue for 61.5 at -99.9 m and 61 s at -86.5 m. With $a = 1.5$ and 2 m, the queue appears for 60.5 s and 78.5 s, respectively, as shown in Figure 9d,e, so the 51st vehicle is in the queue for 60.5 s at -93.2 m and 78.5 s at -86.5 m. With $a = 2.2$ m, the

queue appears for 88.5 s, as shown in Figure 9f, so the 51st vehicle is in the queue for 88.5 s at −89.9 m.

Table 7. Position of the 1st, 30th, and 40th vehicles at 60 s for the ID model.

Acceleration Exponent, δ	1st Vehicle Position (m)	30th Vehicle Position (m)	40th Vehicle Position (m)
1	1230	141.0	−57.6
4	1475	137.1	−72.3
10	1529	207.0	−63.2
30	1553	173.0	−52.2

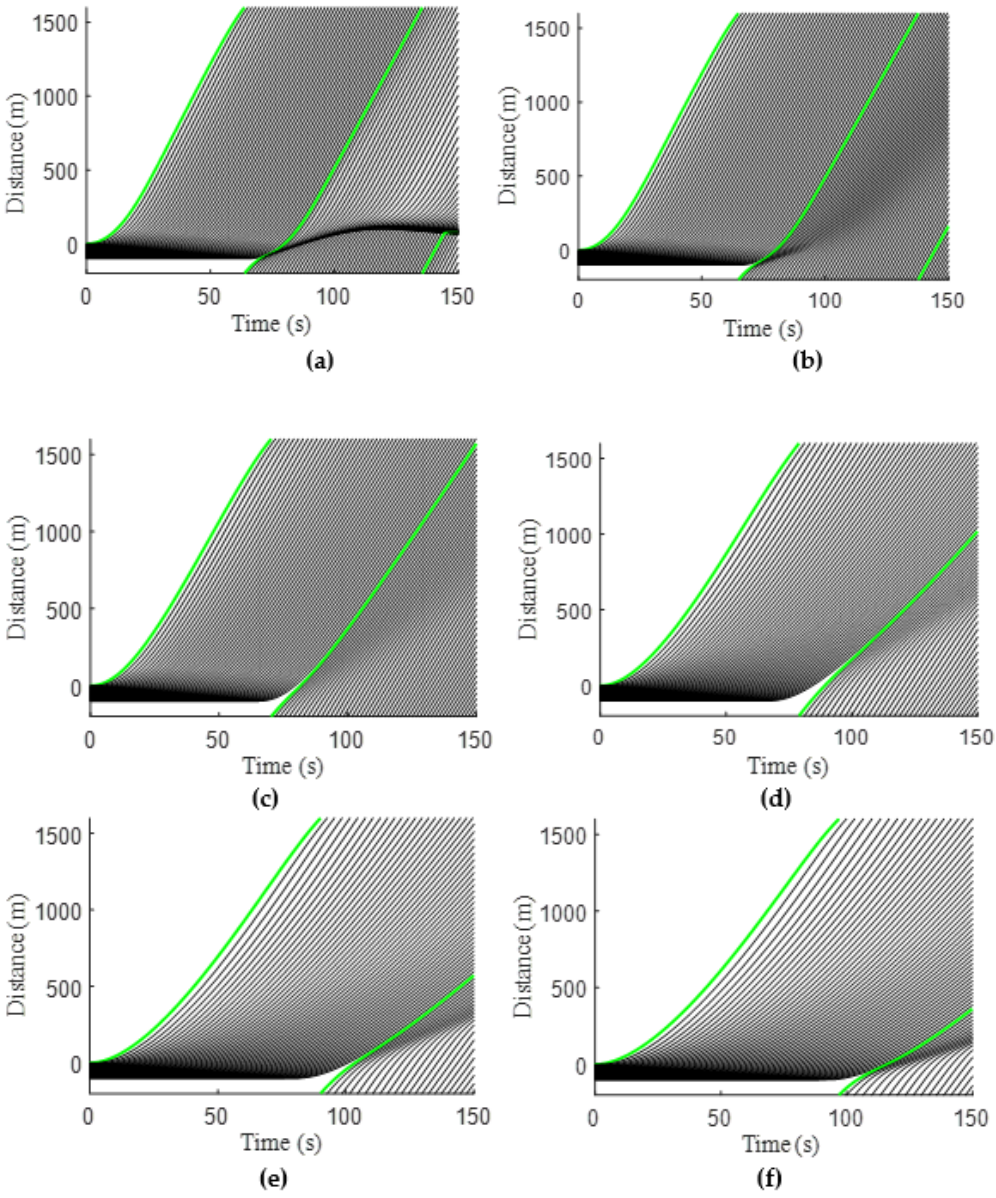

Figure 9. Time–space vehicle trajectories for the proposed model over an 1800 m circular road: (**a**) $a = 0.5$ m; (**b**) $a = 0.6$ m; (**c**) $a = 1$ m; (**d**) $a = 1.5$ m; (**e**) $a = 2$ m; (**f**) $a = 2.2$ m. The colored line shows the trajectory of the first vehicle.

The positions of the 1st, 30th, and 40th vehicles at 60 s are given in Table 8. With $a = 0.5$ m, the position of the 1st vehicle is 1510 m, whereas the positions of the 30th and

40th vehicles are 205.5 m and −39.1 m, respectively. With $a = 0.6$ m, the position of the 1st vehicle is 1485 m, whereas the positions of the 30th and 40th vehicles are 201.5 m and −24.1 m, respectively. With $a = 1$ m, the position of the 1st vehicle is 1351 m, whereas the positions of the 30th and 40th vehicles are 163.3 m and −26.8 m, respectively. With $a = 1.5$ m, the position of the 1st vehicle is 1134 m, whereas the positions of the 30th and 40th vehicles are 80.2 m and −37.8 m, respectively. With $a = 2$ m, the position of the 1st vehicle is 922.3 m, whereas the positions of the 30th and 40th vehicles are −11.0 m and −79.9 m, respectively. With $a = 2.2$ m, the position of the 1st vehicle is 817.3 m, whereas the positions of the 30th and 40th vehicles are −80.0 m and −90.0 m, respectively. Table 8 indicates that as a increases, the distance traveled by the 1st and 30th vehicles decreases. The distance traveled by the 40th vehicle increases between $a = 0.5$ m and 0.6 m but decreases between $a = 1$ m and 2.2 m.

Table 8. Positions of the 1st, 30th, and 40th vehicles at 60 s for the proposed model.

Lateral Distance Headway, a (m)	1st Vehicle Position (m)	30th Vehicle Position (m)	40th Vehicle Position (m)
0.5	1510	205.5	−39.1
0.6	1485	201.5	−24.1
1	1351	163.3	−26.8
1.5	1134	80.2	−37.8
2	922.3	−11.0	−79.9
2.2	817.3	−80.0	−90.0

The temporal evolution of the acceleration for the ID model with $\delta = 1$, 4, 10, and 30 is given in Figure 10. With $\delta = 1$, the acceleration at 8 s is 1.0 m/s^2. It then decreases to −0.45 m/s^2 at 71.5 s and increases to 0.08 m/s^2 at 105.5 s. It decreases to 0.06 m/s^2 at 118 s and is approximately constant until 150 s. With $\delta = 4$, the acceleration at 8.5 s is 1.3 m/s^2. It then decreases to 0.11 m/s^2 at 33.5 s and −1.67 m/s^2 at 67 s. It increases to 1.1 m/s^2 at 81.5 s and decreases to 0.04 m/s^2 at 104.5 s, and is approximately constant until 150 s. With $\delta = 10$, the acceleration at 15 s is 1.38 m/s^2. It then decreases to 0.10 m/s^2 at 29 s and −1.67 m/s^2 at 62 s, and is approximately constant until 72.5 s. It increases to 1.3 m/s^2 between 74.5 s and 85 s and decreases to −0.001 m/s^2 between 101.5 and 134.5 s. It decreases to −1.67 m/s^2 at 141.5 s and is approximately constant until 150 s. With $\delta = 30$, the acceleration at 18 s is 1.37 m/s^2. It then decreases to 0.01 m/s^2 at 27 s and −1.67 m/s^2 at 60 s, and is approximately constant until 72 s. It increases to 1.3 m/s^2 between 74.5 s and 90 s and decreases to −0.001 m/s^2 between 98.5 s and 134.5 s. It then decreases to −1.67 m/s^2 at 139.5 s and is approximately constant until 150 s.

The temporal evolution of acceleration for the proposed model with $a = 0.5$, 0.6, 1, 1.5, 2, and 2.2 m is given in Figure 11. With $a = 0.5$ m, the acceleration at 11.5 s is 1.38 m/s^2. It then decreases to 0.07 m/s^2 at 32 s and −1.67 m/s^2 at 63.5 s, and is approximately constant until 71.5 s. It increases to 1.28 m/s^2 at 81 s and decreases to 0.032 m/s^2 at 101.5 s and 0.001 m/s^2 at 135.5 s. It then decreases to −1.67 m/s^2 at 144.5 s and is approximately constant until 150 s. With $a = 0.6$ m, the acceleration at 9.0 s is 1.38 m/s^2. It then decreases to 0.01 m/s^2 at 37 s and −1.67 m/s^2 at 65.5 s, and then it is approximately constant until 68.5 s. It increases to 1.1 m/s^2 at 81.5 s and decreases to 0.02 m/s^2 at 106.5 s and −0.001 m/s^2 at 149.5 s. With $a = 1$ m, the acceleration at 2 s is 1.38 m/s^2. It then decreases to −0.08 m/s^2 at 50.5 s and −0.82 m/s^2 at 68 s. It increases to 0.4 m/s^2 at 86.5 s and then decreases to 0.1 m/s^2 at 103 s and 0.029 m/s^2 at 125 s, and is approximately constant until 150 s. With $a = 1.5$ m, the acceleration at 0.5 s is 1.4 m/s^2. It then decreases to 0.09 m/s^2 at 51.5 s and −0.27 m/s^2 at 68.5 s. It decreases to −0.4 m/s^2 at 87 s and increases to 0.05 m/s^2 at 106.5 s and 0.087 m/s^2 at 125 s, and is approximately constant until 150 s. With $a = 2$ m, the acceleration at 0.5 s is 1.4 m/s^2. It then decreases to 0.4 m/s^2 at 18.5 s and −0.01 m/s^2 at 69.5 s. It decreases to −0.5 m/s^2 at 94.5 s and increases to 0.1 m/s^2 at 117 s. It then decreases again to 0.06 m/s^2 at 147.5 s and is approximately constant until 150 s. With $a = 2.2$ m, the acceleration at 0.5 s is

1.4 m/s^2. It then decreases to 0.5 m/s^2 at 12.5 s and -0.02 m/s^2 at 74.5 s. It decreases to -0.66 m/s^2 at 99 s, increases to 0.1 m/s^2 at 118 s, and then decreases to 0.05 m/s^2 at 150 s.

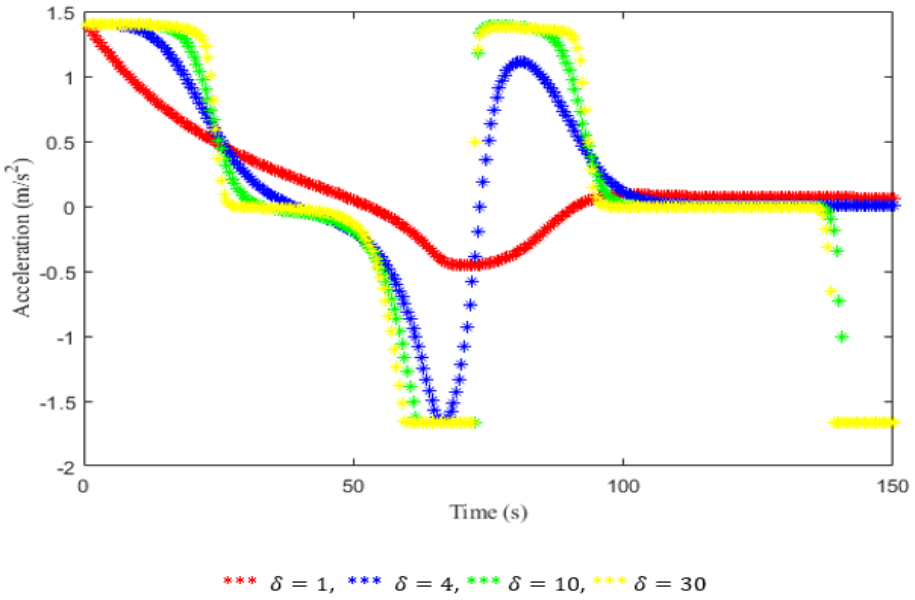

Figure 10. Temporal evolution of acceleration for the ID model.

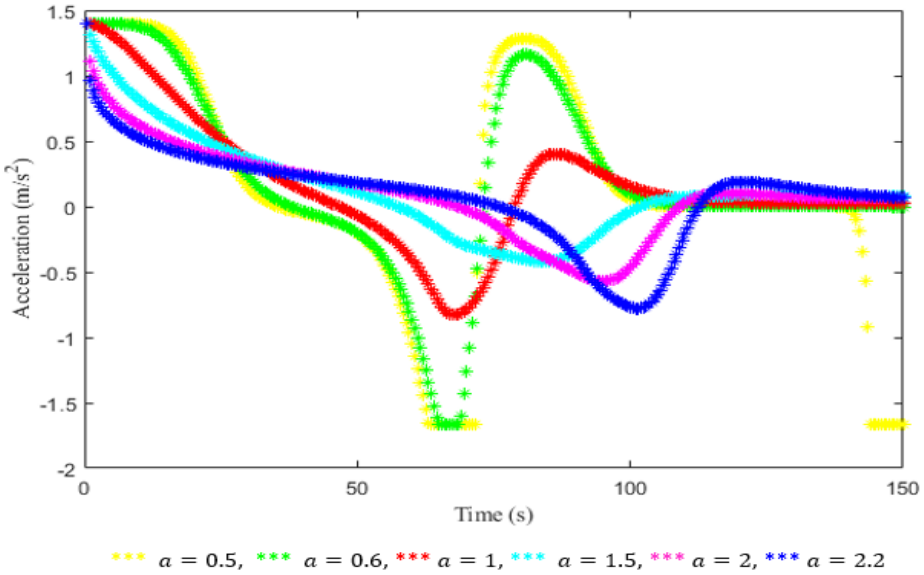

Figure 11. Temporal evolution of acceleration for the proposed model.

The spatio–temporal density behavior of the ID model is given in Figure 12, and the results are summarized in Table 9. With $\delta = 1$, between 0 m and 499.5 m at 150 s, the density is 0.02. It increases to 0.027 at 599.4 m and 0.036 at 789.2 m, then decreases to 0.02 at 1379 m, as shown in Figure 12a. Between 0 s and 62.0 s at -99.9 m, the density is 0.5, which indicates a traffic queue. After the queue dissolves, the density at 65.5 s decreases to 0.06 at -16.7 m. It then decreases to 0.034 at 669.3 m and 149 s. With $\delta = 4$, between 0 m and 409.5 m at 148 s, the density is 0.025. It increases to 0.031 at 782.5 m and then decreases to 0.030 at 1222 m, as shown in Figure 12b. Between 0 s and 61.5 s at -99.9 m, the density is 0.5, which indicates a traffic queue. After the queue dissolves at 75 s, the density decreases to 0.08 at -83.3 m and 0.025 at 409.5 m and 148 s. With δ = 10, between 0 m to 9.99 m at 149.5 s, the density is 0.021. It increases to 0.5 between 16.7 m and 40.0 m, which indicates a traffic queue. It is 0.071 at 83.3 m and decreases to 0.014 at 699.3 m, as shown in Figure 12c.

Between 0 s and 62.5 s, the density is 0.5, which indicates a traffic queue. It then decreases to 0.21 at −96.6 m and 67.5 s. A queue develops again at 72.5 s and −79.92 m with density 0.5, which is approximately constant until 150 s between 16.6 m and 40.0 m. With δ = 30, between 0 m and 10.0 m at 149.5 s, the density is 0.021. It increases to 0.5 between 16.7 m and 40.0 m, which indicates a traffic queue. It is 0.071 at 83.25 m and decreases to 0.014 at 699.3 m, as shown in Figure 12d. Between 0 s and 62.5 s, the density is 0.5, which indicates a traffic queue. The density then decreases to 0.21 at −96.57 m and 67.5 s. A queue develops again at 72.5 s and −79.92 with a density of 0.5, which is approximately constant until 150 s between 16.6 m and 40.0 m.

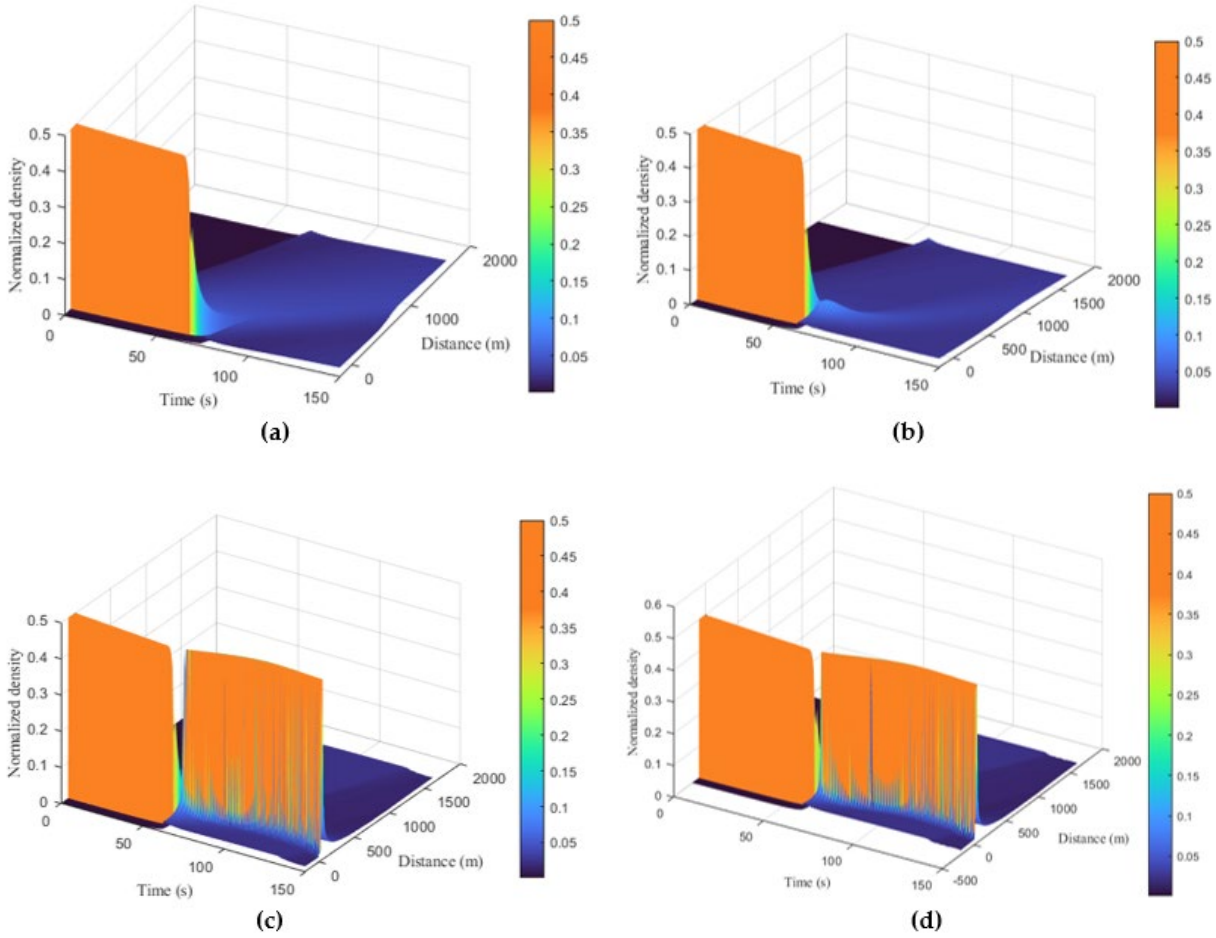

Figure 12. Spatio–temporal density for the ID model over an 1800 m circular road: (**a**) $\delta = 1$; (**b**) $\delta = 4$; (**c**) $\delta = 10$; (**d**) $\delta = 30$.

Table 9. Density and time for the ID model during and after the queue dissolves.

Acceleration Exponent, δ	Time When the Queue Occurs (s)	Density during the Queue	Density after the Queue Dissolves	Time When the Queue Dissolves (s)
1	0–62.0	0.5	0.06	65.5
4	0–61.5	0.5	0.08	75.0
10	0–62.5 and 72.5–150	0.5	0.21	67.5
30	0–62.5 and 72.5–150	0.5	0.21	67.5

The spatio–temporal density behavior of the proposed model is given in Figure 13, and the results are summarized in Table 10. With a = 0.5 m, between 0 m and 53.3 m at 149.5 s, the density is 0.021. It then increases to 0.5 between 66.6 m and 93.2 m, which indicates a traffic queue. It decreases to 0.067 at 129.8 m and 0.015 at 579.4 m, as shown in

Figure 13a. Between 0 s and 57 s, the density is 0.5, which indicates a traffic queue. It then decreases to 0.21 at −96.6 m and 67 s. The queue develops again at 74.5 s and −69.9 m with a density of 0.5 and is approximately constant until 150 s between 66.6 m and 93.2 m. With $a = 0.6$ m, between 0 m and 576.1 m at 149.5 s, the density is 0.027. It increases to 0.036 at 885.7 m and then decreases to 0.029 at 1299 m, as shown in Figure 13b. Between 0 s and 58 s at −99.9 m, the density is 0.5, which indicates a traffic queue. After the queue dissolves, the density decreases to 0.25 at −96.6 m and 66.5 s and 0.11 at −79.9 m and 74.5 s. It is 0.029 at 659.3 m and 148.5 s. With $a = 1$ m, between 0 m and 552.8 m at 148 s, the density is 0.025. It increases to 0.031 at 905.7 m and then decreases to 0.029 at 1329 m, as shown in Figure 13c. Between 0 s and 56.5 s at −99.9 m, the density is 0.5, which indicates a traffic queue. After the queue dissolves, the density decreases to 0.18 at −96.6 m and 67.5 s, and 0.05 at 3.33 m and 79.5 s. It then decreases to 0.031 at 795.8 m and 147 s. With $a = 1.5$ m, between 0 m and 452.8 m at 149.5 s, the density is 0.024. It increases to 0.04 at 662.6 m and then decreases to 0.036 at 852.5 m and to 0.025 at 1489 m, as shown in Figure 13d. Between 0 s and 60 s at −99.9 m, the density is 0.5, which indicates a traffic queue. After the queue dissolves, the density decreases to 0.22 at −96.6 m and 69 s, 0.06 at −6.66 m and 83.5 s, and 0.04 at 596.1 m and 148.5 s. With $a = 2$ m, between 0 m and 126.5 m at 148.5 s, the density is 0.016. It increases to 0.05 at 316.3 m, and then it decreases to 0.038 at 629.3 m and 0.026 at 1089 m, as shown in Figure 13e. Between 0 s and 71 s at −99.9 m, the density is 0.5, which indicates a traffic queue. After the queue dissolves, the density decreases to 0.19 at −96.57 m and 83 s, 0.054 at 59.9 m and 107 s, and 0.051 at 313.0 m and 149 s. With $a = 2.2$ m, between 0 m and 9.99 m at 150 s, the density is 0.016. It increases to 0.06 at 159.8 m, and then decreases to 0.031 at 769.2 m, 0.038 at 449.5 m, and 0.018 at 1419, as shown in Figure 13f. Between 0 s and 77.5 s at −99.9, the density is 0.5, which indicates a traffic queue. After the queue dissolves, the density decreases to 0.25 at −96.57 m and 93.5 s, 0.07 at −29.97 and 113 s, and 0.06 at 146.5 m and 149 s.

Table 10. Density and time for the proposed model during and after the queue dissolves.

Lateral Distance Headway, a	Time When the Queue Occurs (s)	Density during the Queue	Density after the Queue Dissolves	Time When the Queue Dissolves (s)
0.5	0–57 and 74.5–150	0.5	0.21	67.0
0.6	0–58.0	0.5	0.11	74.5
1	0–56.5	0.5	0.05	79.5
1.5	0–60.0	0.5	0.06	83.5
2	0–71.0	0.5	0.19	83.0
2.2	0–77.5	0.5	0.06	93.5

These results show that the changes in density calculated using the proposed model are small. Density and velocity evolve realistically over time as they are based on the lateral distance headway. The changes in density and velocity calculated using the ID model are based on a constant and increase over time with $\delta = 10$ and 30, whereas they should decrease. Moreover, for values greater $\delta = 10$, the behavior is similar, which is not realistic. Further, vehicles move slowly with a larger δ. With the proposed model, vehicles move based on the lateral distance headway, and they are faster with an increase in this headway. Thus, the flow is smooth with the proposed model and is more realistic than with the ID model. In addition, an increase in the lateral distance headway decreases the variations in acceleration, as expected. With the ID model, an increase in δ increases the variations in acceleration, which is unrealistic traffic behavior.

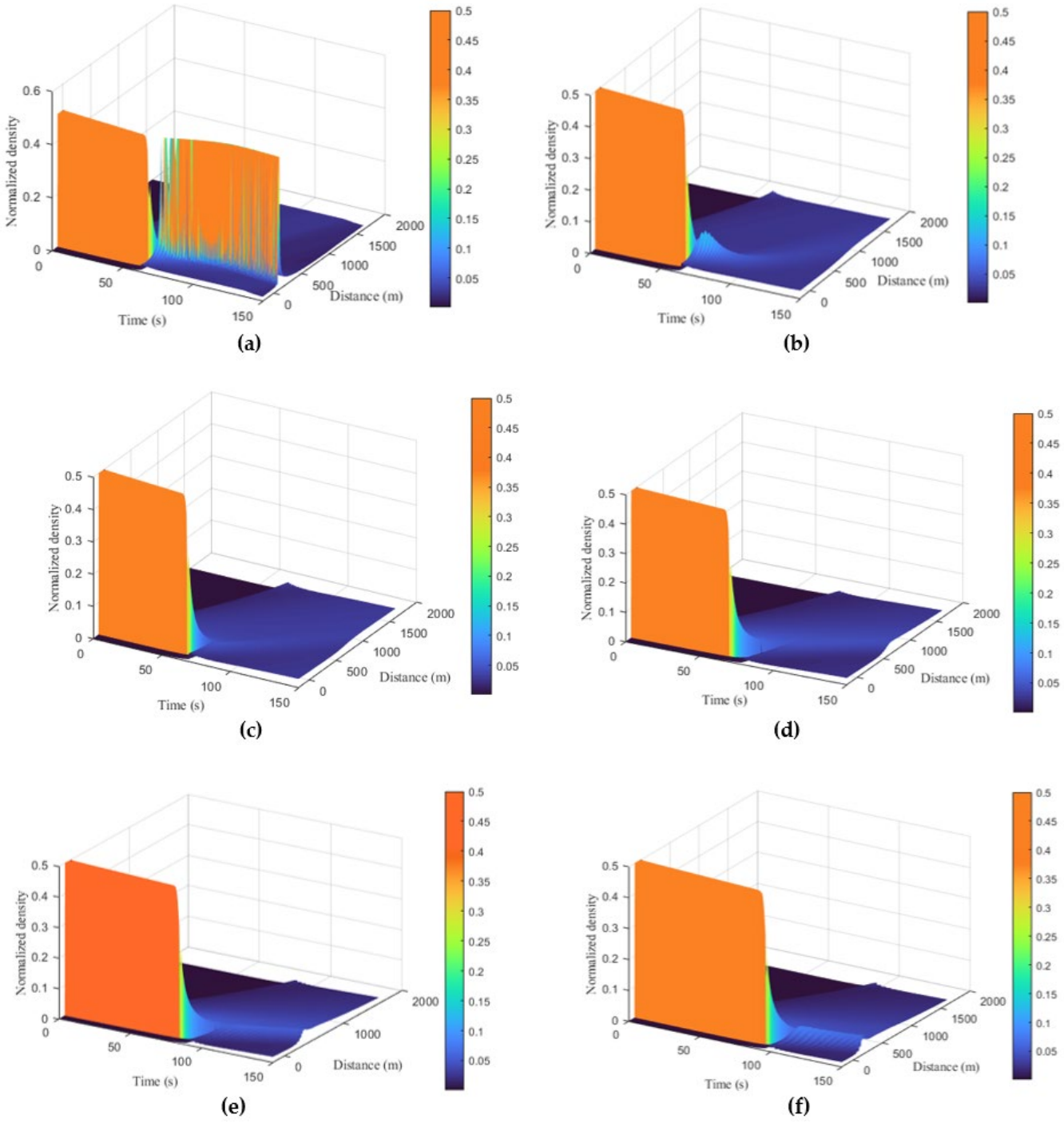

Figure 13. Spatio–temporal density for the proposed model over an 1800 m circular road: (**a**) $a = 0.5$ m; (**b**) $a = 0.6$ m; (**c**) $a = 1$ m; (**d**) $a = 1.5$ m; (**e**) $a = 2$ m; (**f**) $a = 2.2$ m.

5. Conclusions

In this paper, a new heterogeneous traffic model considering the forward and lateral distance headways was proposed. The constant acceleration exponent in the ID model is replaced with an exponent based on realistic traffic parameters to improve the model. It was shown that the ID model produces unrealistic traffic behavior due to a constant exponent. Conversely, the proposed model provides realistic traffic behavior with the velocity and density evolving smoothly over time. Moreover, vehicle movement with the proposed model is faster with a larger lateral distance headway, as expected. With the ID

model, this movement is unrealistic because it is based on a constant. Furthermore, it was shown that the proposed model is more stable than the ID model.

With the proposed model, an increase in the lateral distance headway results in small changes in acceleration compared to the ID model. Large acceleration results in high fuel consumption and an increase in pollution. Hence, the proposed model can be utilized to reduce fuel consumption and pollution due to congestion.

Author Contributions: Conceptualization, F.A. and Z.H.K.; methodology, F.A.; software, F.A and A.N.K.; validation, F.A., Z.H.K., K.S.K. and T.A.G.; formal analysis, F.A., Z.H.K., K.S.K. and T.A.G.; investigation, F.A., Z.H.K. and K.S.K.; writing—original draft preparation, F.A.; writing—review and editing, F.A., Z.H.K., K.S.K. and T.A.G.; visualization, F.A., Z.H.K., K.S.K. and T.A.G.; funding acquisition, Z.H.K., K.S.K. and T.A.G. All authors have read and agreed to the published version of the manuscript.

Funding: This research received no external funding.

Conflicts of Interest: The authors declare no conflict of interest.

References

1. Timilsina, G.R.; Dulal, H.B. Urban road transportation externalities: Costs and choice of policy instruments. *World Bank Res. Obs.* **2011**, *26*, 162–191. [CrossRef]
2. Chung, K.; Rudjanakanoknad, J.; Cassidy, M.J. Relation between traffic density and capacity drop at three freeway bottlenecks. *Transp. Res. Methodol.* **2007**, *41*, 82–95. [CrossRef]
3. Yuan, K.; Knoop, V.L.; Leclercq, L.; Hoogendoorn, S.P. Capacity drop: A comparison between stop-and-go wave and standing queue at lane-drop bottleneck. *Transp. Transp. Dyn.* **2017**, *5*, 145–158. [CrossRef]
4. Rao, A.M.; Rao, K.R. Measuring urban traffic congestion-a review. *Int. J. Traffic Transp. Eng.* **2012**, *2*, 286–305.
5. Carlson, R.C.; Papamichail, I.; Papageorgiou, M. Local feedback-based mainstream traffic flow control on motorways using variable speed limits. *IEEE Trans. Intell. Transp. Syst.* **2011**, *12*, 1261–1276. [CrossRef]
6. Ali, F.; Khan, Z.H.; Khan, F.A.; Khattak, K.S.; Gulliver, T.A. A new driver model based on driver response. *Appl. Sci.* **2022**, *12*, 5390. [CrossRef]
7. Mallikarjuna, C.; Tharun, B.; Pal, D. Analysis of the lateral gap maintaining behavior of vehicles in heterogeneous traffic stream. *Procedia Soc. Behav. Sci.* **2013**, *104*, 370–379. [CrossRef]
8. Imran, W.; Khan, Z.H.; Gulliver, T.A.; Khattak, K.S.; Nasir, H. A macroscopic traffic model for heterogeneous flow. *Chin. J. Phys.* **2020**, *63*, 419–435. [CrossRef]
9. Khan, Z.H.; Imran, W.; Azeem, S.; Khattak, K.S.; Gulliver, T.A.; Aslam, M.S. A macroscopic traffic model based on driver reaction and traffic stimuli. *Appl. Sci.* **2019**, *9*, 2848. [CrossRef]
10. Adebisi, A. *A Review of the Difference among Macroscopic, Microscopic and Mesoscopic Traffic Models*; Florida Agricultural and Mechanical University: Tallahassee, FL, USA, 2017.
11. Khan, Z.H.; Gulliver, T.A.; Khattak, K.S. A novel macroscopic traffic model based on distance headway. *Civ. Eng. J.* **2021**, *7*, 32–40. [CrossRef]
12. Khan, Z.H.; Gulliver, T.A.; Nasir, H.; Rehman, A.; Shahzada, K. A macroscopic traffic model based on driver physiological response. *J. Eng. Math.* **2019**, *115*, 21–41. [CrossRef]
13. Gazis, D.C.; Herman, R.; Rothery, R.W. Nonlinear follow-the-leader models of traffic flow. *Oper. Res.* **1961**, *9*, 545–567. [CrossRef]
14. Newell, G.F. Nonlinear effects in the dynamics of car following. *Oper. Res.* **1961**, *9*, 209–229. [CrossRef]
15. Treiber, M.; Hennecke, A.; Helbing, D. Congested traffic states in empirical observations and microscopic simulations. *Phys. Rev.* **2000**, *62*, 1805–1824. [CrossRef] [PubMed]
16. Newell, G.F. A simplified car-following theory: A lower order model. *Transp. Res. Methodol.* **2002**, *36*, 195–205. [CrossRef]
17. Bando, M.; Hasebe, K.; Nakayama, A.; Shibata, A.; Sugiyama, Y. Dynamical model of traffic congestion and numerical simulation. *Phys. Rev.* **1995**, *51*, 1035–1042. [CrossRef]
18. Helbing, D.; Tilch, B. Generalized force model of traffic dynamics. *Phys. Rev.* **1998**, *58*, 133–138. [CrossRef]
19. Gipps, P.G. A behavioural car-following model for computer simulation. *Transp. Res.* **1981**, *15*, 105–111. [CrossRef]
20. Cao, Z.; Lu, L.; Chen, C.; Chen, X.U. Modeling and simulating urban traffic flow mixed with regular and connected vehicles. *IEEE Access* **2021**, *9*, 10392–10399. [CrossRef]
21. Dahui, W.; Ziqiang, W.; Ying, F. Hysteresis phenomena of the intelligent driver model for traffic flow. *Phys. Rev.* **2007**, *76*, 2–8. [CrossRef]
22. Kesting, A.; Treiber, M.; Helbing, D. Enhanced intelligent driver model to access the impact of driving strategies on traffic capacity. *Philos. Trans. R. Soc. Math. Phys. Eng. Sci.* **2010**, *368*, 4585–4605. [CrossRef] [PubMed]
23. Liebner, M.; Baumann, M.; Klanner, F.; Stiller, C. Driver intent inference at urban intersections using the intelligent driver model. In Proceedings of the IEEE Intelligent Vehicle Symposium, Madrid, Spain, 3–7 June 2012.

24. Derbel, O.; Peter, T.; Zebiri, H.; Mourllion, B.; Basset, M. Modified intelligent driver model for driver safety and traffic stability improvement. *IFAC Proc.* **2013**, *46*, 744–749. [CrossRef]
25. Li, Y.; Li, Z.; Wang, H.; Wang, W.; Xing, L. Evaluating the safety impact of adaptive cruise control in traffic oscillations on freeways. *Accid. Anal. Prev.* **2017**, *104*, 137–145. [CrossRef] [PubMed]
26. De Winter, J.C.F.; Happee, R.; Martens, M.H.; Stanton, N.A. Effects of adaptive cruise control and highly automated driving on workload and situation awareness: A review of the empirical evidence. *Transp. Res. Psychol. Behav.* **2014**, *27*, 196–217. [CrossRef]
27. Jafaripournimchahi, A.; Cai, Y.; Wang, H.; Sun, L.; Weng, J. Integrated-hybrid framework for connected and autonomous vehicles microscopic traffic flow modelling. *J. Adv. Transp.* **2002**, *2022*, 2253697. [CrossRef]
28. Lu, X.; Wang, Z.; Xu, M.; Chen, W.; Deng, Z. A personality model for animating heterogeneous traffic behaviors. *Comput. Animat. Virtual Worlds* **2014**, *25*, 361–371. [CrossRef]
29. Gao, Z.; Wang, J.; Zhang, X.; Dong, J.; Chen, L.; Yan, X.; Zhang, W. Traffic oscillations mitigation in vehicle platoon using a car-following control model for connected and autonomous vehicle. *J. Adv. Transp.* **2019**, *2019*, 3067291. [CrossRef]
30. Dey, P.P.; Chandra, S.; Gangopadhyay, S. Simulation of mixed traffic flow on two-lane roads. *J. Transp. Eng.* **2008**, *134*, 361–369. [CrossRef]
31. Gunay, B. Car following theory with lateral discomfort. *Transp. Res. Methodol.* **2007**, *41*, 722–735. [CrossRef]
32. Metkari, M.; Budhkar, A.; Maurya, A.K. Development of simulation model for heterogeneous traffic with no lane discipline. *Procedia Soc. Behav. Sci.* **2013**, *104*, 360–369. [CrossRef]
33. Mohan, R.; Ramadurai, G. Heterogeneous traffic flow modelling using second-order macroscopic continuum model. *Phys. Lett.* **2017**, *381*, 115–123. [CrossRef]
34. Stern, R.E.; Cui, S.; Delle Monache, M.L.; Bhadani, R.; Bunting, M.; Churchill, M.; Hamilton, N.; Pohlmann, H.; Wu, F.; Piccoli, B.; et al. Dissipation of stop-and-go waves via control of autonomous vehicles: Field experiments. *Transp. Res. Emerg. Technol.* **2018**, *89*, 205–221. [CrossRef]
35. Hu, X.; Chiu, Y.C.; Ma, Y.L.; Zhu, L. Studying driving risk factors using multi-source mobile computing data. *Int. J. Transp. Sci. Technol.* **2015**, *4*, 295–312. [CrossRef]
36. Malinauskas, R. The Intelligent Driver Model: Analysis and Application to Adaptive Cruise Control. Ph.D. Thesis, Clemson University, Clemson, SC, USA, 2014.
37. Kessels, F. *Traffic Flow Modelling: Introduction to Traffic Flow Theory through a Genealogy of Models*; Springer: Cham, Switzerland, 2019.
38. Khansari, E.R.; Tabibi, M.; Nejad, F.M. A study on following behavior based on the time headway. *J. Kejuruter.* **2020**, *32*, 187–195.
39. Toledo, T.; Koutsopoulos, H.N.; Ben-Akiva, M. Integrated driving behavior modeling. *Transp. Res. Emerg. Technol.* **2007**, *15*, 96–112. [CrossRef]
40. Imran, W.; Khan, Z.H.; Gulliver, T.A.; Khattak, K.S.; Saeed, S.; Aslam, M.S. Macroscopic traffic flow characterization for stimuli based on driver reaction. *Civ. Eng. J.* **2021**, *7*, 1–13. [CrossRef]